Four Novel Tarantula Toxins as Selective Modulators of Voltage-Gated Sodium Channel Subtypes[S]

Frank Bosmans, Lachlan Rash, Shunyi Zhu,[1] Sylvie Diochot, Michel Lazdunski, Pierre Escoubas, and Jan Tytgat

Institut de Pharmacologie Moléculaire et Cellulaire Centre National de la Recherche Scientifique Unité Mixte de Recherche 6097, Valbonne, France (L.R., S.D., M.L., P.E.); and Laboratory of Toxicology, University of Leuven, Leuven, Belgium (F.B., S.Z., J.T.)

ABSTRACT

Four novel peptide toxins that act on voltage-gated sodium channels have been isolated from tarantula venoms: ceratotoxins 1, 2, and 3 (CcoTx1, CcoTx2, and CcoTx3) from *Ceratogyrus cornuatus* and phrixotoxin 3 (PaurTx3) from *Phrixotrichus auratus*. The pharmacological profiles of these new toxins were characterized by electrophysiological measurements on six cloned voltage-gated sodium channel subtypes expressed in *Xenopus laevis* oocytes ($Na_v1.1/\beta_1$, $Na_v1.2/\beta_1$, $Na_v1.3/\beta_1$, $Na_v1.4/\beta_1$, $Na_v1.5/\beta_1$, and $Na_v1.8/\beta_1$). These novel toxins modulate voltage-gated sodium channels with properties similar to those of typical gating-modifier toxins, both by causing a depolarizing shift in gating kinetics and by blocking the inward component of the sodium current. PaurTx3 is one of the most potent peptide modulators of voltage-gated sodium channels described thus far from spider venom, modulating $Na_v1.2$ with an IC_{50} value of 0.6 ± 0.1 nM. CcoTx1 and CcoTx2, differing by only one amino acid, are potent modulators of different voltage-gated sodium channel subtypes from the central nervous system, except for $Na_v1.3$, which is only affected by CcoTx2. The potency of CcoTx3 is lower, although this toxin seems to be more selective for the tetrodotoxin-resistant channel subtype $Na_v1.5/\beta_1$ ($IC_{50} = 447 \pm 32$ nM). In addition to these results, molecular modeling indicates that subtle differences in toxin surfaces may relate to their different pharmacological profiles. Furthermore, an evolutionary trace analysis of these toxins and other structurally related three-disulfide spider toxins provides clues for the exploration of toxin-channel interaction and future structure-function research.

Voltage-gated sodium channels (VGSCs) are vital components of cellular function because they participate in the generation and propagation of action potentials. They are composed of a pore-forming α subunit associated with up to four known different β subunits. The α subunits are classified according to sequence homology as $Na_v1.1$ to $Na_v1.9$ and a less defined subunit is called Na_x (Yu and Catterall, 2003; Yu et al., 2003). They are further characterized by their sensitivity to tetrodotoxin (TTX). $Na_v1.5$, $Na_v1.8$, and $Na_v1.9$ are TTX-resistant (TTX-r) and the other α-subunits are TTX-sensitive (TTX-s). Subtype localization varies: $Na_v1.1$, $Na_v1.2$, and $Na_v1.3$ are principally found in the central nervous system, whereas $Na_v1.6$, $Na_v1.7$, $Na_v1.8$, and $Na_v1.9$ are mostly distributed in the peripheral nervous system. $Na_v1.4$ can be found in skeletal muscle, and $Na_v1.5$ is present predominantly in cardiac muscle (French and Terlau, 2004). VGSC dysfunction can result in neuromuscular diseases, including periodic paralysis and heart or brain disorders such as epilepsy (Head and Gardiner, 2003). Mutations in the genes encoding for $Na_v1.1$ and $Na_v1.2$ have been linked to such forms of epilepsy as generalized epilepsy with febrile seizures and severe myoclonic epilepsy of infancy. In some

ABBREVIATIONS: VGSC, voltage-gated sodium channel; TTX, tetrodotoxin; TTX-r, tetrodotoxin-resistant; TTX-s, tetrodotoxin-sensitive; ICK, inhibitory cystine knot; DRG, dorsal root ganglion; RP, reversed phase; HPLC, high-performance liquid chromatography; TFA, trifluoroacetic acid; MALDI-TOF, matrix-assisted laser desorption ionization/time of flight; TEVC, two-electrode voltage-clamp; PDB, Protein Data Bank; HnTx, hainantoxin; PaurTx, phrixotoxin; CcoTx, ceratotoxin; I-V, current-voltage; SNX482, Ca^{2+} channel-blocking toxin from *Hysterocrates gigas* spider venom.

demyelinating diseases, defective nerve conduction occurs and involves up-regulation of Na$_v$1.2 (Craner et al., 2004). Cardiac channelopathies, including arrhythmias such as the long QT syndrome 3, Brugada syndrome, progressive cardiac conduction defect, and familial nonprogressive conduction defect have been linked to mutations in Na$_v$1.5 (Head and Gardiner, 2003). Finally, the demonstration that VGSC subtypes such as Na$_v$1.3, Na$_v$1.7, Na$_v$1.8, and Na$_v$1.9 are involved in pain pathways has made them attractive targets for the development of novel therapeutic strategies for pain treatment (Julius and Basbaum, 2001; Nassar et al., 2004). For instance, neuropathic pain resulting from peripheral nerve damage has been linked with overexpression of Na$_v$1.3 and is currently insufficiently addressed by analgesics (Wood et al., 2004).

As crucial components of the development of action potentials, VGSCs are one of the foremost targets of animal venoms or plant neurotoxins (Possani et al., 1999; Bosmans et al., 2002; Lewis and Garcia, 2003; French and Terlau, 2004). Toxins from various organisms have been used to describe eight different receptor sites on the α subunit of VGSCs, all of which are linked to specific effects on channel function (Wang and Wang, 2003). However, toxin characterization is often limited to whole-cell sodium currents and binding studies on neuronal membranes. For most of these toxins, the precise pattern of subtype selectivity is either unknown or at best fragmentary.

In the past 2 years, a number of novel spider toxins have been demonstrated to modulate VGSCs (Escoubas and Rash, 2004). Although the overall structure of these toxins, based on the inhibitory cystine knot (ICK) fold, is fairly similar, their electrophysiological properties vary greatly (Escoubas et al., 2000b; Rash and Hodgson, 2002; Sollod et al., 2005). Hainantoxins I, II, IV, and V as well as huwentoxin IV do not alter activation or inactivation kinetics (Li et al., 2003, 2004; Peng et al., 2002). They reduce the current amplitude and have therefore been hypothesized to act by occluding the ion conduction pathway, similarly to toxins acting on site 1. Conversely, the protoxins and jingzhaotoxin-III shift the activation voltage toward more positive values, without affecting inactivation (Middleton et al., 2002; Xiao et al., 2004). The protoxins inhibit several VGSC subtypes but can also hamper the function of selected voltage-gated calcium or potassium channels. At this moment, the exact site of action of these toxins on the VGSC α subunit remains the object of speculation. It is thought that they bind to DII-S3/DII-S4 near site 4.

To find more selective modulators of different VGSCs subtypes, we have screened a large number of tarantula venoms on six cloned VGSC subtypes and investigated the activity of the four most potent toxins purified from two of those venoms. To examine potential promiscuous action of the toxins, we also tested them on mouse DRG neurons as a source of voltage-gated calcium channels and on K$_v$1.3 as a representative voltage-gated potassium channel. Mouse central injections allowed us to examine their overall neurotoxicity pattern. To complement our pharmacological analysis, homology modeling and an evolutionary trace (ET) analysis of these new peptides and other structurally related spider toxins were performed. The results reported here offer new insights into the mode of action of this family of VGSC modulators and the associated structure-function relationships.

Materials and Methods

Spider Venoms. *Ceratogyrus cornuatus* (Cco) and *Phrixotrichus auratus* (Paur) venoms were purchased from a commercial supplier (Invertebrate Biologics, Los Gatos, CA). Venom was collected from groups of adult female specimen by electrical stimulation of chelicerae and was then freeze-dried. Dried samples (dry weight ~20% of volume) were redissolved in distilled water to 10 times the initial venom volume (1:10 dilution), centrifuged (14,000 rpm, 20 min), filtered on 0.45-μm microfilters (Millipore Corporation, Billerica, MA) and stored at -20°C.

Toxin Purification. A total of 110 μl of crude *C. cornuatus* venom and 10 μl of crude *P. auratus* venom was fractionated by C8 reversed-phase semipreparative HPLC (10 × 250 mm; Nacalai Tesque, Kyoto, Japan) using a linear gradient of water (A)/acetonitrile (B) in constant 0.1% trifluoroacetic acid (0–15% B in 15 min, 15–50% in 70 min, 50–60% in 10 min, 60–90% in 10 min, 2 ml/min). Fractions were hand-collected by monitoring the effluent signal (215 nm) and dried in a vacuum centrifuge. Aliquots of each fraction were assayed for activity against cloned VGSCs expressed in *Xenopus laevis* oocytes (see below). Active fractions were further separated by cation-exchange chromatography on an SP5PW column (4.6 × 70 mm) (TOSOH, Tokyo, Japan), with a linear gradient of ammonium acetate in water from 20 mM (A) to 2 M (B) (0% B for 10 min, 0–60% in 60 min, 60–95% B in 10 min, 1 ml/min, detection at 280 nm). A third purification step was conducted for each active peak using a C4 reversed-phase column (Develosil 300C4, 4.6 × 250 mm, Nomura Chemical, Seto, Japan) and a linear gradient of acetonitrile in water and 0.1% TFA (0% B for 5 min, 0–40% in 80 min, 40–90% in 10 min, 1 ml/min). All solvents used were of HPLC grade. Separations were conducted on a HP1100 system (Hewlett Packard, Palo Alto, CA) coupled to a diode-array detector.

Toxin Characterization. For N-terminal sequence determination, peptides were reduced (55 mM dithiothreitol, 60°C, 1 h) and alkylated with iodoacetamide (RT, 30 min), desalted by reversed-phase high performance liquid chromatography (RP-HPLC) on a Purospher STAR column (C18, 55 × 4 mm, 3 μm; Merck, Whitehouse Station, NJ) (water/acetonitrile/0.1% TFA, 0–40% B in 20 min, 1 ml/min) and submitted to automated N-terminal sequencing on a gas-phase sequencer (model 477A; Applied Biosystems, Foster City, CA).

For confirmation of the sequences and sequencing of the C terminus, reduced and alkylated peptides were digested with trypsin (500 pmol of peptide, trypsin ratio of 1:50 (w/w) in 25 mM NH$_4$HCO$_3$ buffer, pH 8.3, 12 h at 37°C). After quenching the reaction with 0.1% TFA in water, an aliquot was analyzed by MALDI-TOF mass spectrometry, and the mixture of proteolytic peptides was separated by reversed-phase HPLC on the same analytical column (water/acetonitrile/0.1% TFA, 0–60% B in 60 min, 1 ml/min). Each fraction was then analyzed by MALDI-TOF mass spectrometry. Peptides corresponding to the unknown part of the sequence according to mass calculations done in GPMAW (http://welcome.to/GPMAW) were submitted to automated Edman sequencing.

Sequence similarities were determined by a search of nonredundant protein databases, via the BLAST server (http://www.ncbi.nlm.nih.gov/) and by comparison with sequences obtained from literature data and compiled in an in-house spider peptide toxin database. Sequence alignments were calculated using ClustalX 1.8.

Mass Spectrometry. Peptides were analyzed by MALDI-TOF mass spectrometry on an Applied Biosystems Voyager DE-PRO system, in reflector mode using recrystallized α-cyano-4-hydroxycinnamic acid matrix. Mass spectra were calibrated with internal peptide standards and analyzed in the Data Explorer software. Masses were also measured by electrospray ionization on a Thermo Finnigan LCQ DecaXP electrospray ion trap mass spectrometer (Thermo Electron Corporation, Waltham, MA).

Mouse Intracerebroventricular Injections. Activity against vertebrates was evaluated by i.c.v. injection in mice. C57/Bl6 mice

were briefly anesthetized with diethyl ether, injected in the left cerebral ventricle with 10 μl of sample (500 pmol of toxin in 10 μl of double-distilled H_2O) or control (10 μl double-distilled H_2O) and placed in glass jars for observation. Mice were continuously monitored for symptoms of neurotoxicity during the first hour after injection or until death. All the experiments involving the use of animals complied with University Ethics Regulations.

DRG Preparation and Patch-Clamp Recording of Calcium Currents. Dorsal root ganglia (DRG) were dissected from adult mice (7–10 weeks) and enzymatically dissociated with collagenase (0.2% type II; Worthington Biochemicals, Freehold, NJ) and trypsin (2.5 mg/ml; Seromed, Berlin, Germany). Cells were plated on 35-mm Petri dishes coated with poly-(L-lysine) (Sigma, St. Louis, MO) and maintained in culture at 37°C (95% air/5% CO_2) in Ham's F12 medium (Invitrogen, Carlsbad, CA) containing 10% fetal calf serum (MP Biomedicals, Irvine, CA) and 1% penicillin/streptomycin (Invitrogen). Electrophysiological experiments were carried out 1 or 2 days after plating.

Currents were sampled at 3.3 kHz for whole-cell recordings using pClamp8 software (Molecular Devices, Sunnyvale, CA). The pipette solution contained 150 mM CsCl, 1 mM $MgCl_2$, 5 mM EGTA, 3 mM ATP, and 10 mM HEPES-CsOH, pH 7.35, and the bath solution contained: 140 mM TEACl, 5 mM $BaCl_2$, 10 mM glucose, and 10 mM HEPES-TEAOH, pH 7.35. Solutions were applied near the neuron using a rapid perfusion system. The holding potential was −80 mV and high voltage-activated calcium currents were elicited by depolarizing steps between −20 and +50 mV. Averaged data are presented as mean ± S.E.M.

Sodium Channel Expression. For expression in *X. laevis* oocytes, the $Na_v1.5$ and β_1 genes were previously subcloned into pSP64T. For in vitro transcription, $Na_v1.5$/pSP64T and $Na_v1.8$/pSP64T were first linearized with XbaI and β_1/pSP64T with EcoRI. Capped cRNAs were synthesized from the linearized plasmid using the SP6 mMESSAGE mMACHINE transcription kit (Ambion, Austin, TX). The $Na_v1.1$/pLCT1, $Na_v1.2$/pLCT1, $Na_v1.3$/pNa3T, and $Na_v1.4$/pUI-2 vectors were linearized with NotI and transcribed with the T7 mMESSAGE mMACHINE kit (Ambion) (Kayano et al., 1988; Smith and Goldin, 1998; Bosmans et al., 2002).

Potassium Channel Expression. The vector pCI.neo containing the gene for $K_v1.3$ was linearized with NotI and transcribed using the large-scale T7 mMESSAGE mMACHINE transcription kit (Ambion) (Swanson et al., 1990).

Electrophysiological Studies on Cloned Channels. The harvesting of stage V–VI oocytes from the ovarian lobes of anesthetized female *X. laevis* frogs was done as described previously (Bosmans et

al., 2002). Oocytes were injected with 50 nl of cRNA at a concentration of 1 ng/nl using a microinjector from Drummond Scientific (Broomall, PA). The solution used for incubating the oocytes contained 96 mM NaCl, 2 mM KCl, 1.8 mM $CaCl_2$, 2 mM $MgCl_2$, and 5 mM HEPES, pH 7.4, supplemented with 50 mg/l gentamycin sulfate and 180 mg/l theophylline.

Two-electrode voltage-clamp (TEVC) recordings were performed at room temperature (18–22°C) using a GeneClamp 500 amplifier (Molecular Devices) controlled by a pClamp data acquisition system (Molecular Devices). Whole-cell currents from oocytes were recorded 2 to 4 days after injection. Voltage and current electrodes were filled with 3 M KCl. Resistances of both electrodes were kept as low as possible (<0.5 MΩ). Bath solution composition was 96 mM NaCl, 2 mM KCl, 1.8 mM $CaCl_2$, 2 mM $MgCl_2$, and 5 mM HEPES, pH 7.4. Currents were filtered at 1 kHz with a four-pole, low-pass Bessel filter and sampled at 5 kHz. Leak subtraction was performed using a −P/4 protocol. Currents were evoked in oocytes expressing the cloned VGSCs by depolarizations between −70 and 40 mV, using 10-mV increments from a holding potential of −90 mV. To avoid overestimation of a potential toxin-induced shift in the current-voltage relationship as a result of inadequate voltage control when measuring large sodium currents in oocytes, only results from cells with currents lower than 1.5 μA were considered in Table 1. To obtain IC_{50} values on VGSCs, the percentage of toxin-induced block was plotted against the concentration of toxin used and a fit with the Hill equation yielded the IC_{50} values. The percentage of toxin-induced block was always measured at the same voltage, which also gave the maximum current under control conditions (no toxin: *). This method was preferred over choosing a fixed voltage (e.g., −20 mV) for all VGSCs to avoid a distorted calculation of toxin-induced block of channels that activate at more positive voltages (e.g., $Na_v1.8$). Furthermore, over the tested voltage range (between −20 and +30 mV), the percentage of toxin-induced block, compared among all the VGSC isoforms, was found to be invariable [data derived from Fig. 4 (not shown)]. $K_v1.3$ currents were evoked by depolarizations to 0 mV from a holding potential of −90 mV. All toxins were tested on at least three oocytes ($n \geq 3$). Data manipulation was performed in pClamp8 (Molecular Devices) and Origin software (OriginLab Corp., Northampton, MA). Averaged data are presented as mean ± S.E.M.

Molecular Modeling. Three-dimensional models of phrixotoxin (PaurTx) 3, ceratotoxin (CcoTx) 1, and CcoTx2 were calculated using the NMR structure coordinates of hainantoxin IV [HnTx-IV; Protein Data Base (PDB) code 1NIY] as a template, whereas the model for CcoTx3 was calculated using the hanatoxin 1 structure (PDB code

TABLE 1

Numerical overview of the obtained data

To obtain IC_{50} values on VGSCs, the percentage of toxin-induced block was plotted against the concentration of toxin used. A fit with the Hill equation (see Fig. 2) provided the IC_{50} values (Hill coefficient between brackets). For the IC_{50} values, the percentage of toxin-induced block was always measured at the same voltage that gave the maximum current obtained under control conditions. All toxins were tested on at least three oocytes ($n \geq 3$). Averaged data are presented as mean ± S.E.M. A representative example of the shift in $V_{1/2}$ is also provided for all toxins. A positive number indicates a significant shift of the I-V curve to more positive potentials compared with $V_{1/2}$ in control conditions. Only $\Delta V_{1/2}$ values of sodium currents lower than 1.5 μA are considered.

	CcoTx1	CcoTx2	CcoTx3	PaurTx3
IC_{50} values (maximal toxin addition is 2 μM)				
$Na_v1.1/\beta_1$	523 ± 79 nM (0.9)	407 ± 36 nM (1.4)	N.A.	610 ± 63 nM (0.9)
$Na_v1.2/\beta_1$	3 ± 1 nM (1.3)	8 ± 1 nM (1.1)	N.A.	0.6 ± 0.1 nM (1.0)
$Na_v1.3/\beta_1$	N.A.	88 ± 25 nM (1.8)	N.A.	42 ± 4 nM (1.1)
$Na_v1.4/\beta_1$	888 ± 80 nM (1.0)	400 ± 54 nM (1.3)	N.A.	288 ± 58 nM (1.5)
$Na_v1.5/\beta_1$	323 ± 56 nM (1.5)	1634 ± 133 nM (1.0)	447 ± 32 nM (1.7)	72 ± 10 nM (1.5)
$Na_v1.8/\beta_1$	55% block	40% block	45% block	65% block
$\Delta V_{1/2}$ values (representative sodium currents <1.5 μA)				
$Na_v1.1/\beta_1$	+1.7 mV	+5.3 mV	—	+1.9 mV
$Na_v1.2/\beta_1$	+14.3 mV	+17.0 mV	—	+10.7 mV
$Na_v1.3/\beta_1$	+7.5 mV	+5.1 mV	—	+10.2 mV
$Na_v1.4/\beta_1$	+19.8 mV	+20.5 mV	+10.4 mV	+5.9 mV
$Na_v1.5/\beta_1$	+6.1 mV	+9.1 mV	+1.5 mV	+12.9 mV
$Na_v1.8/\beta_1$	—	—	—	—

NA, no activity; —, no significant shift of $V_{1/2}$.

1D1H). The templates were selected among available experimentally determined structures, for identical cysteine positions and the highest possible primary sequence homology to minimize the number of possible side-chain rotamer positions. Initial backbone fitting and energy minimization steps were performed with the DeepView program (Swiss-PDB Viewer, http://www.expasy.ch/spdv/) and further refined via submission to the Swiss-Model server (http://www.expasy.ch/swissmod/SWISS-MODEL.html). Estimation of model reliability, calculation of electrostatic potentials and model exploration were carried out using DeepView (http://www.expasy.org/spdbv).

Evolutionary Trace Analysis. The sequences of 33 inhibitory spider venom peptides conforming to the ICK fold were used in the evolutionary trace analysis (Craik et al., 2001). These sequences are supplied online as a Supplemental Table. The multiple sequence alignment was performed using the program ClustalX and was manually refined. The ET analysis was carried out based on a phylogenetic tree created with the unweighted pair group method with arithmetic mean. To summarize briefly, the ET method divides all residues of aligned sequences into three classes: neutral, conserved,

and class-specific, based on the comparison of consensus sequences for groups of proteins that originate from a common node defined by the evolutionary time cut-off in a phylogenetic tree (for details, see Zhu et al., 2004). Class-specific trace residues identified were mapped onto the structure of HnTX-IV (PDB code 1NIY) in the PyMOL molecular modeling program (http://pymol.sourceforge.net).

Results

Toxin Purification and Characterization. In the initial screening of ~20 tarantula venoms, both *C. cornuatus* and *P. auratus* venoms consistently displayed high and reproducible inhibitory activity against a variety of cloned VGSCs. The bioassay-guided fractionation of *C. cornuatus* venom resulted in the identification of three active fractions. Two peptides were isolated from fraction 24 and fraction 25/26 yielded another one, which were named, respectively, CcoTx1, CcoTx2, and CcoTx3) (see Fig. 1A). Bioassay-guided
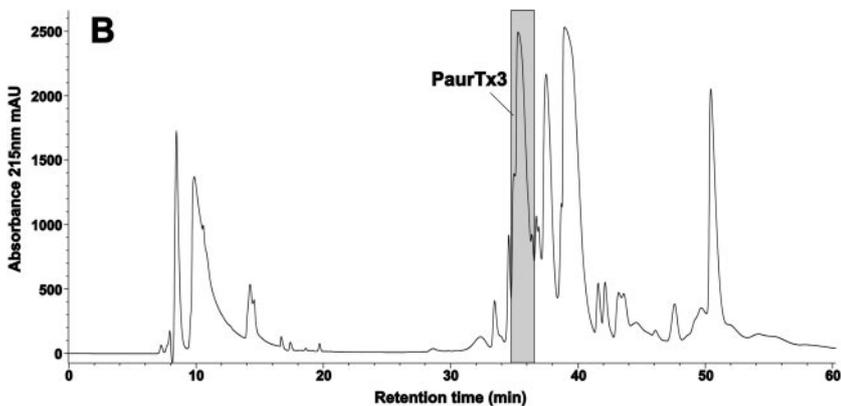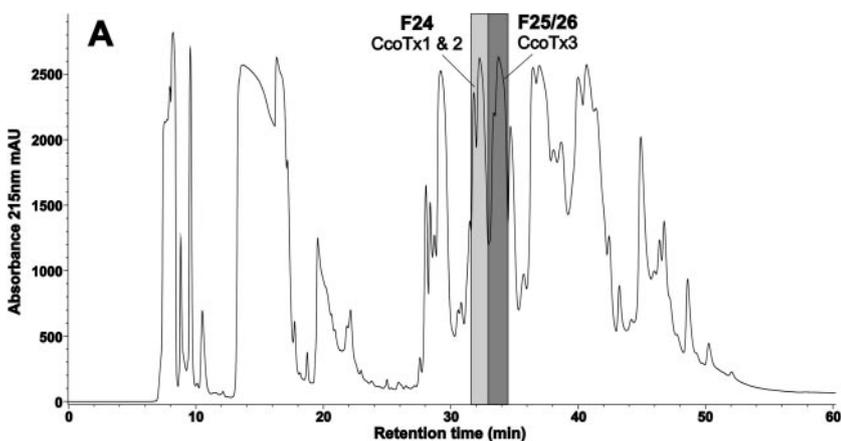

Fig. 1. Initial purification and sequences of the ceratotoxins and phrixotoxin 3. A, initial RP-HPLC separation of crude *C. cornuatus* venom (50 μl) with a linear gradient of water/acetonitrile in constant 0.1% TFA. Fractions 24 and 25/26 were further purified to obtain CcoTx1/CcoTx2 and CcoTx3, respectively (see *Materials and Methods* for details). B, initial RP-HPLC separation of crude *P. auratus* venom (10 μl) with a linear gradient of water/acetonitrile in constant 0.1% TFA. The arrow indicates the peak, which was further purified to yield PaurTx3. C, ClustalW sequence alignments of CcoTx1–3 and PaurTx3 with other closely related toxins isolated from tarantula venoms: HnTxIV (*S. hainana*; Xiao and Liang, 2003), HwTxIV (*O. huwena*; Peng et al., 2002), GsMTx4 (*G. spatulata*; Suchyna et al., 2000), HnTxIII (*S. hainana*; Xiao and Liang, 2003), SNX482 (*H. gigas*; Newcomb et al., 1998), hanatoxin 1 (*G. spatulata*) (Swartz and MacKinnon, 1995), SGTx1 (*Scodra griseipes*; Wang et al., 2004), and ProTx1 (*Thrixopelma pruriens*) (Middleton et al., 2002). Amino acid numbering and percentage similarity are shown relative to CcoTx1 (top alignment) and CcoTx3 (bottom alignment).

fractionation of *P. auratus* venom yielded a single active peptide named PaurTx3 (see Fig. 1B). Purity of the toxins (>99%) was assessed in the last two steps of purification using orthogonal methods (ion-exchange followed by reversed-phase), which yielded single, symmetrical peaks, and by MALDI-TOF mass spectrometry, which did not reveal the presence of contaminants. Automated sequencing of all reduced and alkylated peptides yielded almost complete sequences and sequencing of several overlapping tryptic peptides completed the C-terminal part of the sequences.

The four toxins are 32 to 39 amino acids long, and they each possess six cysteine residues forming three disulfide bridges (based on molecular mass data). CcoTx1, CcoTx2 and PaurTx3 are basic peptides (respective calculated pI 10.48, 10.07, 10.18) and CcoTx3 is an acidic peptide (pI 6.05). The molecular masses measured by MALDI-TOF mass spectrometry (PaurTx3, 4055.88 Da; CcoTx1, 4041.79 Da; CcoTx2, 4089.61 Da; and CcoTx3, 4321.84 Da) are in perfect accordance with those calculated from the sequence data. They indicate amidation at the C terminus of CcoTx1 (calc. 4041.74 Da), CcoTx2 (calc. 4089.78 Da), and CcoTx3 (calc. 4321.85 Da) (−1 Da difference with the molecular mass calculated with a carboxylic C terminus). Likewise, mass spectrometry indicates a free carboxyl-terminal form for PaurTx3 (calc. 4055.87 Da).

CcoTx1, CcoTx2, and PaurTx3 are highly similar toxins; CcoTx1 and CcoTx2 are isoforms that are different only at position 32, with an aspartic acid residue in CcoTx1 and a tyrosine in CcoTx2. CcoTx3 shows a completely different primary sequence. The pairing of cysteine residues was not determined experimentally in the present study, because the very high similarity of the ceratotoxins and phrixotoxin 3 with toxins described previously strongly suggests that they conform to the canonical motif $C_I–C_{IV}$, $C_{II}–C_V$, $C_{III}–C_{VI}$ found in all members of this structural group (Escoubas and Rash, 2004). Our sequences were analyzed with CysView, a web-based tool that identifies and classifies proteins according to their disulfide connectivity patterns (http://research.i2r.a-star.edu.sg/CysView). The results returned by the program suggested that CcoTx1, CcoTx2, CcoTx3, and PaurTx3 indeed adhere to the aforementioned disulfide bridge canonical motif.

Sequence Similarity. CcoTx1, CcoTx2, and PaurTx3 share a high similarity with other peptides previously isolated from other tarantula venoms (Fig. 1C). The most similar toxins are Huwentoxin IV (74%, 74%, and 77%) and Hainantoxin IV (77%, 75%, and 82%), VGSC inhibitors from the Chinese tarantulas *Ornithoctonus huwena* and *Selenocosmia hainana*, respectively (Peng et al., 2002; Li et al., 2004), and GsMTX4 (74% for PaurTx3), an inhibitor of mechanosensitive channels from the venom of the Chilean tarantula *Grammostola spatulata* (Suchyna et al., 2000).

CcoTx3 shares a high similarity with toxin SNX482 (76%), an R-type voltage-gated calcium channel blocker from the African tarantula *Hysterocrates gigas* (Newcomb et al., 1998) and with the $K_v2.1$ channel inhibitor hanatoxin 1 (60%) from the venom of *G. spatulata* (Swartz and MacKinnon, 1995) (see Fig. 1C).

Mouse Neurotoxicity. Mice injected with 500 pmol of CcoTx1, CcoTx2, and PaurTx3 displayed exactly the same symptoms of neurotoxicity: injection of the toxins was immediately followed by general ataxia, lack of response to stimuli,

and semiparalysis. After a few minutes, the mice were unable to stand, and breathing was reduced in rhythm and intensity. Symptoms gradually increased with progressive slowing of breathing and flaccid paralysis; death occurred within 10 to 20 min of injection. Animals remained totally flaccid, and during the course of intoxication, no symptoms of excitatory neurotoxicity (spasms, convulsions, rapid movements) were observed. Conversely, CcoTx3 injection resulted in markedly different symptoms characterized by an erect, elevated tail, initial partial ataxia, followed by recovery over approximately 1 h after injection and the progressive development of shaking. Although paralysis subsided, the body tremors never ceased and persisted until the end of the experiment.

Activity on Calcium Currents. Using the whole cell configuration of the patch-clamp technique on sensory neurons from adult mice, high-voltage activated (HVA) calcium currents were activated between −20 and +50 mV from a holding potential of −80 mV to obtain current-voltage relationships (I-V curves). Perfusion of CcoTx1, CcoTx2, CcoTx3, and PaurTx3 at 100 nM concentration did not inhibit HVA calcium currents evoked at −10 or 0 mV in sensory neurons (2.4 ± 3, 4 ± 4, 10 ± 7, and 2.5 ± 5% inhibition, respectively, $n = 4$ each) (data not shown).

Activity on Sodium Currents. Using the TEVC technique on *Xenopus laevis* oocytes, the effects of CcoTx1, CcoTx2, CcoTx3, and PaurTx3 were compared on six different cloned VGSCs coexpressed with the β_1 subunit ($Na_v1.1/\beta_1$, $Na_v1.2/\beta_1$, $Na_v1.3/\beta_1$, $Na_v1.4/\beta_1$, $Na_v1.5/\beta_1$, and $Na_v1.8/\beta_1$) (see Figs. 2 and 3, Table 1). Clones for $Na_v1.6$ and $Na_v1.7$ were not available at the time of this study and the $Na_v1.9$ channel currently fails to express in heterologous systems. When measured at the voltage of maximum sodium influx, CcoTx1 decreases $Na_v1.1$, $Na_v1.2$, $Na_v1.4$, and $Na_v1.5$ currents with variable potency. At the maximum concentration tested (2 μM), there is no observable inhibition of $Na_v1.3$ and only ~55% inhibition of $Na_v1.8$. CcoTx1 seems to be very highly selective for the neuronal channel $Na_v1.2$, with an IC_{50} value of 3 ± 1 nM, whereas IC_{50} values for the other subtypes are at least 2 orders of magnitude higher. The I-V curves of all TTX-s VGSCs are shifted to more positive potentials when CcoTx1 is applied, and voltage of half-maximal activation ($V_{1/2}$) increases substantially (see Table 1). $Na_v1.1$ is influenced to a lesser degree ($V_{1/2}$, +1.7 mV), and the I-V curve of $Na_v1.8$ displays no shift at all.

CcoTx2, which differs by only one amino acid from CcoTx1 (D32Y), reduces the current of all studied VGSCs with different potencies but reduces $Na_v1.8$ current only by ~40% at a concentration of 2 μM. CcoTx2 is similar to CcoTx1 in that it displays the strongest inhibition on $Na_v1.2$.

The most striking result concerning CcoTx1 and CcoTx2 is the dramatic effect of the single mutation of Asp32 to Tyr32 on $Na_v1.3$ activity. Whereas CcoTx1 elicits no observable inhibition of this particular subtype, $Na_v1.3$ current is inhibited by CcoTx2 with an IC_{50} of 88 ± 25 nM, pointing at the crucial role of this C-terminal residue in channel subtype selectivity.

PaurTx3, the most potent toxin in our study, affects all studied VGSCs with different IC_{50} values (see Table 1). Here again, $Na_v1.8$ is the least sensitive to the toxin, with a current reduction of ~65% at a concentration of 2 μM. PaurTx3 is particularly potent against $Na_v1.2$ (IC_{50} = 0.6 ± 0.1 nM)

and is also by far the most potent toxin for $Na_v1.5$ in our study (IC$_{50}$ = 72 ± 10 nM). As with CcoTx1 and CcoTx2, PaurTx3 is much less potent against $Na_v1.1$ (IC$_{50}$ = 610 ± 63 nM) and $Na_v1.4$ (IC$_{50}$ = 288 ± 58 nM). All I-V curves except the one for $Na_v1.8$ are also shifted to more positive potentials for this toxin (Fig. 4).

No obvious alteration in inactivation rate is observed in all these experiments, and there was also no noticeable shift in reversal potential (E_{rev}), suggesting that toxin interaction with the VGSCs does not cause a change in ion selectivity.

Additional experiments were performed using CcoTx2 to clarify whether these toxins act as pore blockers or gating

modifiers. One of the characteristics of gating modifier toxins is that whereas they mediate complete inhibition of all inward currents, outward currents can still be observed despite the presence of the toxin (McDonough et al., 1997; Bourinet et al., 2001). CcoTx2 (50 nM) apparently changes the voltage dependence of gating of $Na_v1.2/\beta_1$, so channels do not open in response to the moderate depolarizations that evoke inward current through unblocked channels (Fig. 5A). Nevertheless, channels can still be opened by sufficiently large depolarizations to +120 mV. However, a major limitation for studying sodium currents in oocytes is the presence of endogenous outward currents at very positive voltages. We tried to min-
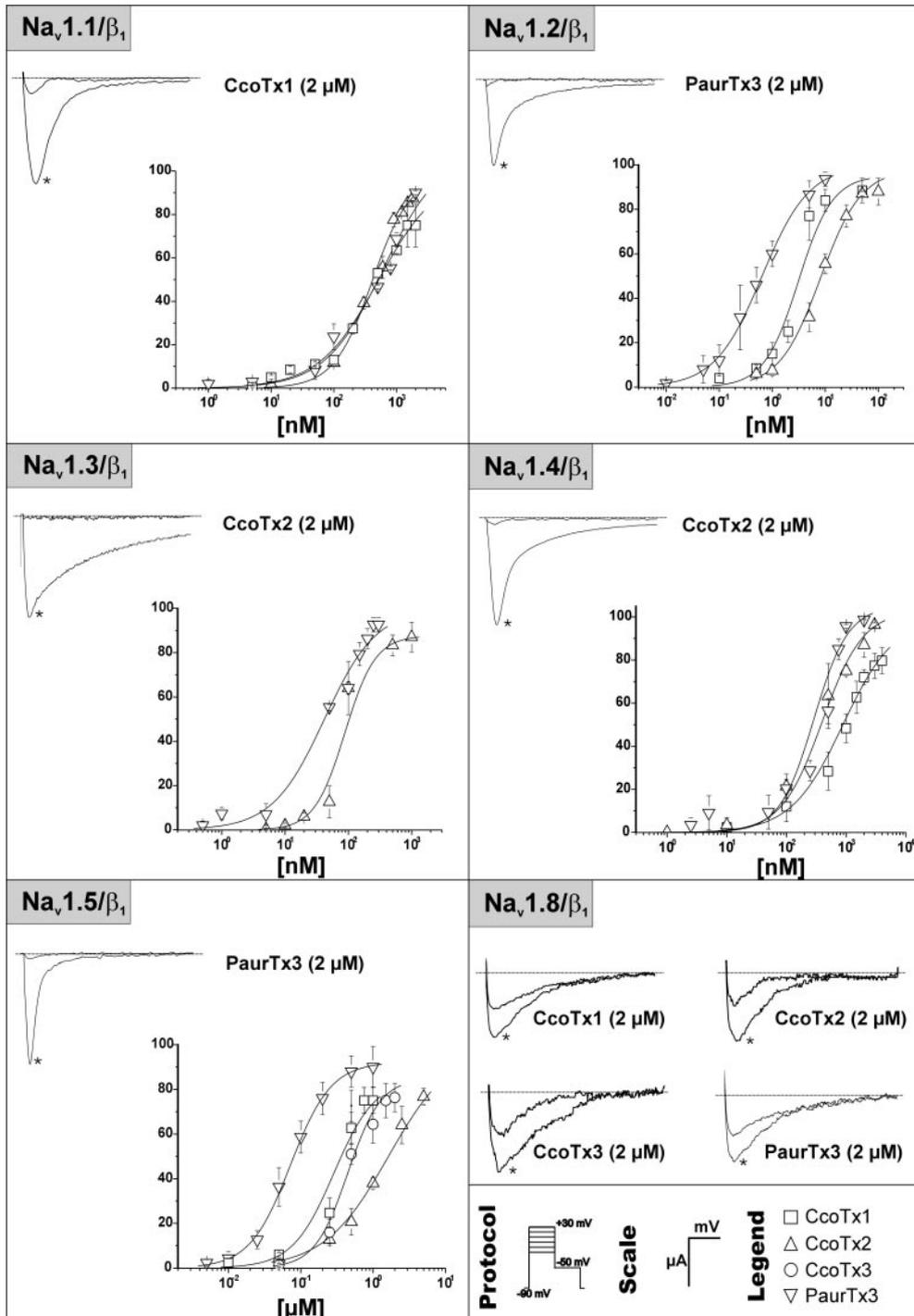
Fig. 2. Effect of the ceratotoxins and phrixotoxin 3 on all studied VGSCs. Current traces were evoked by depolarizations ranging from −20 to +30 mV, depending on the VGSC, from a holding potential of −90 mV. One example trace without (*) and with the most potent toxin (2 μM) is shown per VGSC. Concentration-response curves of all active toxins are shown for each VGSC (y-axis, percentage block) and are the result of a fit (Hill equation) of the obtained data. The percentage of toxin-induced current inhibition was always measured at the same voltage that gave the maximum current obtained under control conditions. Over the tested voltage range (between −20 and +30 mV), the percentage of toxin-induced block, compared among all the VGSC isoforms, was found to be invariable (data derived from Fig. 4). Because all toxins block $Na_v1.8/\beta_1$ only for 40 to 60% at a concentration of 2 μM, no concentration-response curves are shown here. Bottom right corner of the figure shows the protocol, scale of the traces, and legend of the concentration-response curves. Scale bars: x-axis, 5 mV for all traces; y-axis, for $Na_v1.1/\beta_1$, 150 nA; for $Na_v1.2/\beta_1$, $Na_v1.3/\beta_1$, and $Na_v1.4/\beta_1$, 200 nA; for $Na_v1.5/\beta_1$, 600 nA; and for $Na_v1.8/\beta_1$, 100 nA.

imize this effect as shown in Fig. 5B by plotting a trace at $+80$ mV and subtracting the endogenous currents measured on uninjected oocytes at this voltage ($n = 5$). As shown in Fig. 5B, sodium current is still present at $+80$ mV that inactivates over time, and the currents elicited at voltages more positive than the E_{rev} are superimposed in both control and toxin application experiments. To test whether CcoTx2 (50 nM) was still bound to the channel ($Na_v1.2/\beta_1$) after large depolarizations, a test pulse to -10 mV was given 25 ms after a 50-ms depolarization to $+120$ mV (Fig. 5C). The current at -10 mV was still inhibited by CcoTx2 after the large depolarization, which could be interpreted to mean that CcoTx2 was still bound to the channel. We also observed that the rate of development of inhibition upon CcoTx2 exposure occurred with a time constant of >20 s for this cell, which is slow compared with the 25-ms interval between the pulse to $+120$ mV and the start of the second pulse to -10 mV. Thus, it is far more likely that the inhibition during the second pulse to -10 mV reflects continuous presence of CcoTx2 on or nearby the channel throughout the pulse sequence rather than toxin unbinding during the pulse to $+120$ mV followed by rebinding before the following pulse to -10 mV. The trace shown here at $+120$ mV has not been corrected for the presence of endogenous currents at very positive voltages, and therefore an outward current is seen. In the inset, the deactivation of these endogenous currents is displayed.

The application of 2 μM CcoTx3 does not result in current inhibition for $Na_v1.1$, $Na_v1.2$, $Na_v1.3$, or $Na_v1.4$. As with CcoTx1 and CcoTx2, CcoTx3 does reduce $Na_v1.8$ currents by $\sim45\%$. The only VGSC that is somewhat sensitive to CcoTx3 is the TTX-r $Na_v1.5$, with an IC_{50} value of 447 ± 32 nM. In addition, CcoTx3 barely shifts the I-V curve of $Na_v1.5$. In contrast, the I-V curve of $Na_v1.4$ was substantially shifted but only at concentrations of 2 μM or more. The rather low potency of CcoTx3 on the tested VGSCs can probably be attributed to its very different primary sequence and suggests either a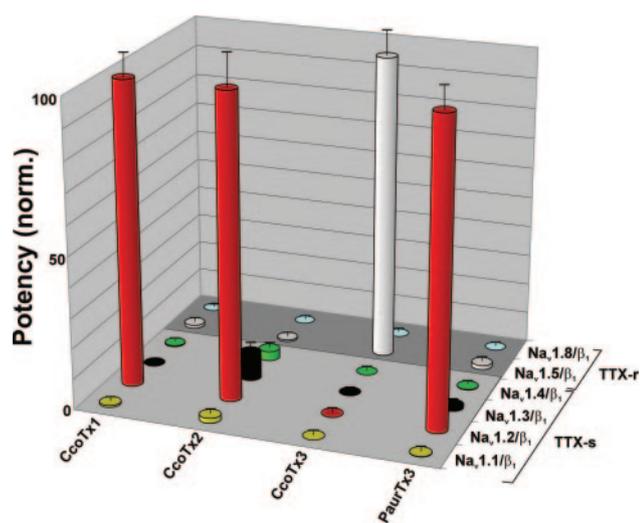 preferential affinity for other pharmacological targets such as calcium channels or potassium channels or selectivity for VGSCs of a different phylogenetic origin.

Activity on Potassium Currents. Using the TEVC technique on *X. laevis* oocytes, the effects of CcoTx1, CcoTx2, CcoTx3, and PaurTx3 were studied on $K_v1.3$, a member of the voltage-gated potassium channel family. Currents were evoked by depolarizations to 0 mV from a holding potential of
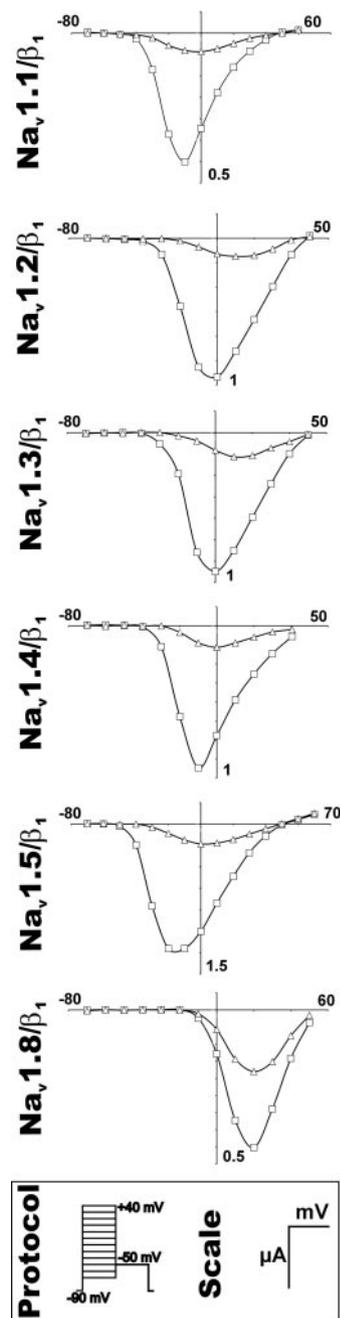

Fig. 4. VGSCs under the influence of the ceratotoxins and phrixotoxin 3 reveal a shift in current-voltage (I-V) relationship. As a representative example, the I-V curves of all studied VGSCs in the presence (2 μM, $\triangle$) or absence ($\square$) of PaurTx3 are shown. To avoid overestimation of the shift due to inadequate voltage control when measuring large sodium currents in oocytes, only results from cells with sodium currents lower than 1.5 μA are shown. The shifts caused by the other toxins are displayed in Table 1. No shift in reversal potential (E_{rev}) is seen. This shift in the I-V relationship of the studied VGSCs (with the exception of $Na_v1.8/\beta_1$) is a trademark that our toxins have in common with ProTx-I, ProTx-II, and jingzhaotoxin-III (Middleton et al., 2002; Xiao et al., 2004).

Fig. 3. Bar diagrams indicating the potencies of the ceratotoxins and phrixotoxin 3. Potencies (IC_{50} values from Table 1) are normalized per toxin. The VGSC, against which the toxin is the most potent, is indicated as 100%. Lower potencies on other VGSCs are represented as a fraction of 100%. CcoTx1, CcoTx2, and PaurTx3 display the highest potency on $Na_v1.2/\beta_1$. CcoTx3 is selective for $Na_v1.5/\beta_1$ although its potency is low. The targeted VGSCs are grouped into TTX-s and TTX-r channels.

−90 mV and then clamped back to −50 mV. Neither CcoTx1, CcoTx2, CcoTx3, nor PaurTx3 had any substantial effect on $K_v1.3$ currents, causing less than 20% block at a concentration of 2 μM ($n = 3$) (data not shown). Extensive testing on other members of the K_v family could not be undertaken because of insufficient material.

Structural Analysis. In accordance with their primary sequence similarity, examination of the models of the four toxins shows that they indeed adopt an ICK fold motif, with backbones closely matching those of other spider toxins studied by NMR (Craik et al., 2001; Escoubas and Rash, 2004). Further examination of the toxin surfaces points out the similarity of the three basic toxins (CcoTx1, CcoTx2, and PaurTx3) with other toxins acting on voltage-gated channels, such as SGTx1, a tarantula toxin inhibiting activation of $K_v2.1$ channels (Lee et al., 2004) (see Fig. 6). These toxins seem to be organized into two distinct faces, with the face interacting with the channel bearing a hydrophobic patch surrounded by a crown of charged residues. The importance of this structural organization in gating-modifier ICK toxins was first proposed by Takahashi et al. (2000) to explain the interaction between hanatoxin and *drk1* ($K_v2.1$). The model was validated in recent mutagenesis studies that singled out the essential role of the hydrophobic protrusion on the surface of SGTx1 (Wang et al., 2004). This protrusion consists of an "aromatic sandwich" encompassing both hydrophobic and two or three aromatic residues. Sequence alignment shows that similar residues can be found in equivalent positions in loop 4 of the ceratotoxins and PaurTx3 between cysteines IV and V. The three-dimensional models show that they form a similar hydrophobic patch on the surface of the molecule. This area is borne by the first N-terminal β-turn and the first two β-sheets of the toxin, stabilized by the disulfide bridges. Hence, the central hydrophobic patch is essentially formed by residues in the second β-sheet (after Cys IV).

In addition, the important role of the single amino acid mutation between CcoTx1 and CcoTx2 demonstrates the crucial importance of the C terminus of the toxin in subtype selectivity. This residue is located on the face of the toxin opposite the hydrophobic patch and therefore highlights the complexity of toxin-channel interaction that does not involve solely the face bearing the hydrophobic patch.

Both the primary sequence and the three-dimensional model of CcoTx3 clearly distinguish it as a different type of ICK toxin. The surface features and in particular the charge distribution of CcoTx3 are very different from those of CcoTx1, CcoTx2, and PaurTx3, clearly reflecting its acidic nature and probable different channel selectivity. In addition, the hydrophobic surface homologous to that of the other ceratotoxins is discontinuous and extends to the C-terminal loop. Its high sequence similarity with SNX482, a blocker of R-type voltage-gated calcium channels, and the results of our
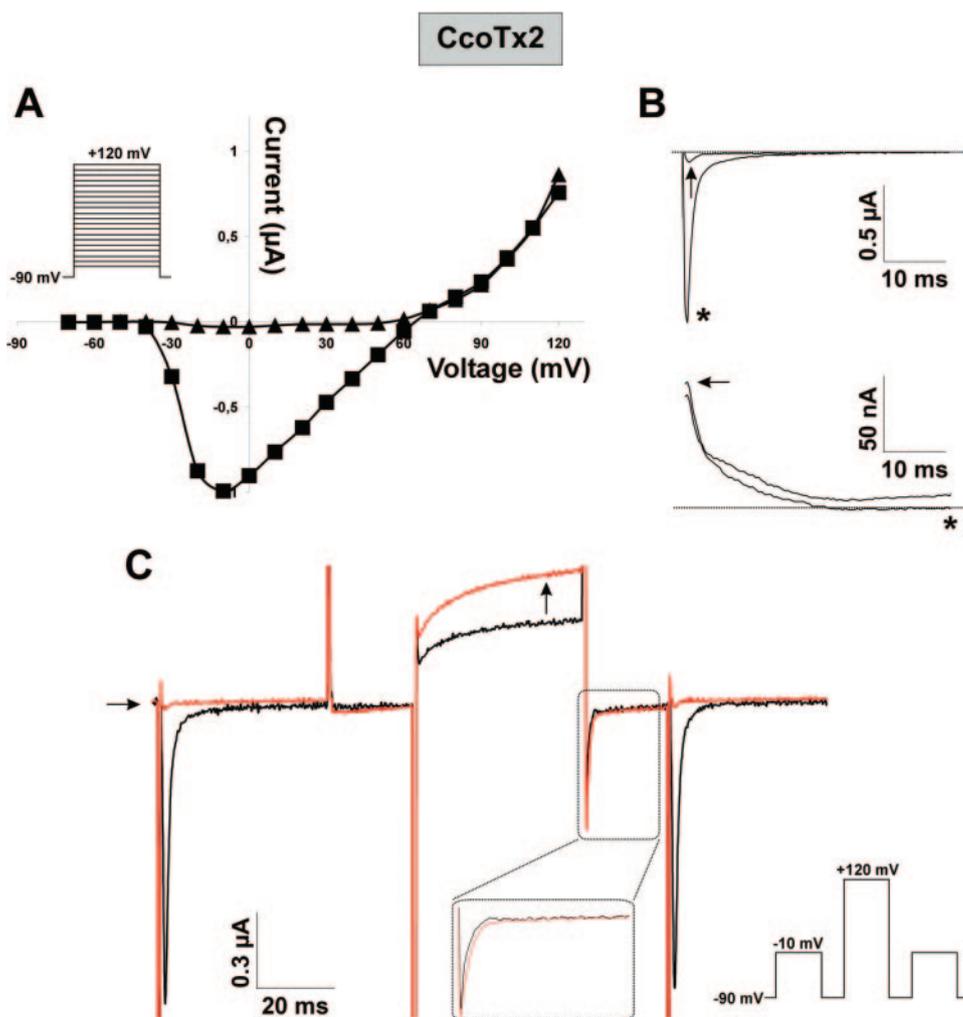
Fig. 5. Gating modification effects of CcoTx2 on $Na_v1.2/\beta_1$. A, CcoTx2 (50 nM) completely blocks inward $Na_v1.2/\beta_1$ currents but not the outward currents, as seen in the current-voltage relationship. B, top trace, the current is evoked by a 50-ms depolarization to −10 mV; bottom trace, the current is evoked by a 50-ms depolarization to +80 mV from a holding potential of −90 mV and corrected by subtracting the endogenous currents of reference oocytes at this voltage ($n = 5$). Outward currents are still observed in the presence of 50 nM CcoTx2. C, CcoTx2 (50 nM) is still bound to the channel after a 50-ms depolarizing pulse to +120 mV (red trace). The trace shown here at +120 mV has not been corrected for the presence of endogenous currents at very positive voltages; therefore, an outward current is seen. Inset, deactivation of these endogenous currents is shown. The protocol used is displayed in the bottom right corner.

electrophysiological study on VGSCs, may point at possible activity against voltage-gated calcium channels. However, no significant inhibition of the HVA calcium currents in DRG neurons was observed. The ultimate target of the peptide might thus be a subtype that is not expressed in this cell model or is responsible only for a minor fraction of the total current. No significant effect was observable on $K_v1.3$ either.

Evolutionary Trace Analysis. To complete this study, a bioinformatics-based investigation of toxin residues that are potentially important in toxin/channel interaction and functional diversification was undertaken. It was based on the evolutionary trace method (ET), which identifies sequence positions at which variations among related proteins correlate with evolutionary divergence. After ET analysis of 33 sequences with a common ICK motif, the amino acids that were calculated as being of significant importance are highlighted in red in Fig. 7. These residues are mapped onto the structure of HnTX-IV (Li et al., 2004). Examination of the three-dimensional model makes it clear that almost all evolutionarily important residues, either structurally or pharmacologically, are located on face A of the toxin. Only a leucine at position 3 is located on face B, which is defined by a 180° rotation of face A around the *y*-axis of the toxin. A remarkable feature is the strong basic node that is present in face A and consists of an arginine (Arg26) and two lysines (Lys27 and Lys32), among which Lys32 is the only significantly important residue located in a β-sheet. Furthermore, it seems that the final loop between the two antiparallel β-sheets is an important functional surface, because four of the six residues in this loop (Ser25, Arg26, Lys27, and Trp30) are highlighted by our ET analysis.

Discussion

Electrophysiology-guided purification of two of the most active venoms in our screening, *C. cornuatus* and *P. auratus,* resulted in the isolation of four novel VGSC toxins. These peptides belong to the "long loop" ICK peptides subgroup (Escoubas and Rash, 2004). Toxins described previously in this family include not only toxins acting on VGSCs but also toxins that inhibit voltage-gated calcium and potassium channels, mechanosensitive cationic channels, and proton-gated ion channels (Swartz and MacKinnon, 1995; Escoubas et al., 2000a; Suchyna et al., 2000; Escoubas et al., 2002; Middleton et al., 2002). In this report, we present for the first time an extensive picture of ICK spider toxin subtype selectivity for VGSCs and demonstrate that selectivity can be finely modulated by subtle structural differences.

Toxins as Tools to Study VGSCs. Both CcoTx1 and CcoTx2 are able to inhibit $Na_v1.2$ inward currents in the low nanomolar range, but display only moderate activity against $Na_v1.1$, $Na_v1.4$, $Na_v1.5$, and low activity against $Na_v1.8$ (Figs. 2, 3, and 5 and Table 1). Their pharmacological profile indicates that these peptides, when used at concentrations near their IC_{50}, could be used to selectively characterize $Na_v1.2$ currents in neurons in which $Na_v1.2$ is coexpressed with $Na_v1.1$ and $Na_v1.3$. While CcoTx2 is an effective modulator of both $Na_v1.2$ ($IC_{50} = 8 \pm 1$ nM) and $Na_v1.3$ ($IC_{50} = 88 \pm 25$ nM), CcoTx1, which differs by only one C-terminal residue, does not inhibit $Na_v1.3$ currents at concentrations
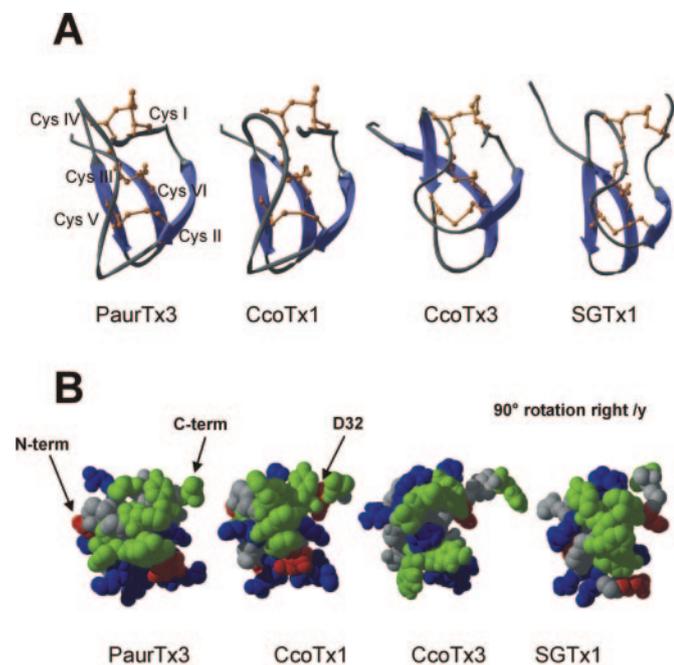

Fig. 6. Molecular modeling and structural features of the ceratotoxins and phrixotoxin 3. A, ribbon representations of calculated models for PaurTx3, CcoTx1, and CcoTx3. The ribbon structure of SGTx1 (PDB code 1LA4) from *S. griseipes*, a representative ICK peptide acting on voltage-gated potassium channels is shown for comparison. Disulfide bridges forming the cystine knot are orange. B, CPK representation of the same peptides after a 90° vertical counterclockwise rotation, showing the common aromatic-hydrophobic patch (green) and the crown of charged residues (basic in blue, acidic in red). Note the similarity of the two VGSC toxins PaurTx3 and CcoTx1 with the voltage-gated potassium channel toxin SGTx1, and the dissimilarity of the aromatic-hydrophobic patch of CcoTx3. Residues are colored according to the scheme proposed by Takahashi et al. (2000).
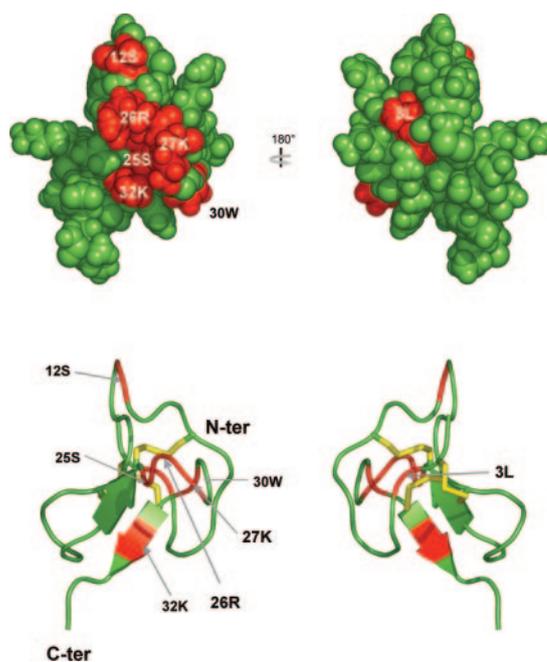

Fig. 7. ET analysis. This bioinformatics-based technique identifies sequence positions at which variations among related proteins always correlate with evolutionary divergence. The obtained evolutionary important residues are mapped onto HNTX-IV (PDB code 1NIY). Striking is the presence of a strong basic node in Face A (left). The final loop between the two anti-parallel β-sheets seems important for pharmacological activity. The 33 sequences with a common ICK motif on which this ET analysis is based are provided as a Supplemental Table.

up to 2 μM. Not only will the combined application of both toxins permit observation of Na$_v$1.1-related currents only, their separate application should also allow discrimination of Na$_v$1.2 from Na$_v$1.3.

With even higher affinity toward Na$_v$1.2, PaurTx3 is a complementary tool for the study of this channel (Figs. 2, 3, and 4 and Table 1). The overall pharmacological profile of PaurTx3 is similar to that of CcoTx2. It inhibits Na$_v$1.2 (IC$_{50}$ = 0.6 $\pm$ 0.1 nM), and it is also the most potent inhibitor of Na$_v$1.5 in our study.

Our results demonstrate the crucial role of the C-terminal part of these peptides in their interaction with the VGSC and especially in recognizing Na$_v$1.3. For the toxins reported here, the presence of either an acidic group (Asp32 in CcoTx1) or an aromatic one (Tyr32 in CcoTx2) dramatically changes the selectivity through a minor change in its overall structure and surface charge (Fig. 6). Similarly to CcoTx2, the C-terminal acidic residue of CcoTx1 (Asp32) is mutated to a polar uncharged residue (Gln32) in PaurTx3. As in CcoTx2, this modification results in affinity toward Na$_v$1.3 and seems to be critical in the recognition of this particular channel, perhaps by the formation of a hydrogen bond network or the presence of the π-electron cloud of the Tyr32 ring.

Although discovered through the same process of bioassay-guided purification, CcoTx3 has the least activity against the tested VGSCs (Figs. 2 and 3 and Table 1). Examination of its primary structure reveals a sequence totally different from that of the other ceratotoxins but closely related to SNX482 (Fig. 1C). It could be hypothesized that CcoTx3 has a different, high-affinity primary target. The bias in activity-guided purification can be explained by the high abundance of the toxin in the venom and possible "target promiscuity" as shown previously for other ion channel spider toxins. It has been demonstrated previously that at elevated concentrations (>500 nM), ion channel selectivity can be modified, with recognition of conserved motifs such as the voltage-sensing domain in other channel families (Li-Smerin and Swartz, 1998). Nevertheless, under certain conditions, CcoTx3 might still be of use in the study of the VGSC family as a selective ligand of moderate affinity for Na$_v$1.5.

Modulation of Channel Function. Application of CcoTx1, CcoTx2, and PaurTx3 results in a shift of the current-voltage relationship of the studied VGSCs (Figs. 4 and 5 and Table 1), a characteristic that has also been reported for related spider toxins such as protoxin I, protoxin II, and Jingzhaotoxin III (Middleton et al., 2002; Xiao et al., 2004; Smith et al., 2005). In those studies, it was assumed that these toxins bind to the extracellular linker between DII-S3 and DII-S4 of the VGSC. A similar modification of ion channel activation was also observed in voltage-gated calcium channels with the spider toxins ω-agatoxin-IVA, ω-grammo-toxin-SIA, and the scorpion toxin kurtoxin (Li-Smerin and Swartz, 1998; Winterfield and Swartz, 2000). These toxins have thus been classified as gating modifiers. However, other related ICK toxins isolated from tarantula venoms, such as hainantoxins I, III, IV, V, and huwentoxin IV have been reported to entirely block sodium currents without affecting either activation or inactivation. They have been classified as pore blockers, acting by occlusion of the channel, in a manner similar to that of site 1 toxins (Li et al., 2003, 2004; Xiao and Liang, 2003). These studies raise the intriguing possibility of

different binding sites and modes of action on the VGSC for these ICK spider toxins.

Our experiments on Na$_v$1.2 using CcoTx2 (Fig. 5) reveal a complete inhibition of all inward currents, but outward currents can still be observed despite the presence of the toxin. Furthermore, as seen in Fig. 5C it seems that CcoTx2 stays continuously bound to or is near the channel even at very positive voltages (+120 mV). In addition, CcoTx1, CcoTx2, and PaurTx3 affect neither channel inactivation nor reversal potential. Compared with certain voltage-gated calcium channel toxins, which have been characterized as gating modifiers, our toxins are quite similar in their mode of action. Both ω-grammotoxin-SIA (McDonough et al., 1997) and SNX482 (Bourinet et al., 2001) completely block inward calcium currents. However, they do not inhibit outward currents. Considering these results, we suggest that the toxins described in the present report can also be generally classified as gating modifiers.

On the other hand, we show that the ceratotoxins and PaurTx3 do not cause a shift of the voltage-current relationship in Na$_v$1.8 (Fig. 4) but rather seem to act in a manner resembling that of pore blockers. One simple hypothesis for this divergent behavior could be that Na$_v$1.8, which already has a much more positive activation potential by itself, does not possess a high sequence similarity with other VGSCs, and therefore lacks a conserved voltage-sensing domain (Li-Smerin and Swartz, 1998; Winterfield and Swartz, 2000). A concomitant supporting fact is that Na$_v$1.8 is also insensitive to the "classic" toxins from scorpions, spider (F. Bosmans and J. Tytgat, unpublished data), and sea anemones (Bosmans et al., 2002).

Because of fragmented data in the literature, it remains difficult to properly compare the "activation blockers" of VGSCs. Both the protoxins and Jingzhaotoxin III have only been reported to block channel activation (Middleton et al., 2002; Xiao et al., 2004). The decrease of inward currents or the binding site of these toxins has not been thoroughly described. A way of classifying our toxins other than as gating modifiers could therefore be as "voltage-dependent blockers", which block only inward sodium currents in a voltage-dependent manner. All the above actually suggests a slightly different mode of action for these peptides and certainly warrants further investigation.

A recent study focused on the molecular surface of tarantula toxins interacting with the voltage sensor of voltage-gated potassium channels (Wang et al., 2004). The authors stated that SGTx1 interacts with the lipid membrane via its hydrophobic protrusion with a crown of surrounding residues containing important residues (Arg3, Arg22) for contacting the voltage sensor. A similar mechanism of partitioning in the lipid membrane was also recently described for ProTx-II (Smith et al., 2005). CcoTx1, CcoTx2, and PaurTx3 possess a similar hydrophobic protrusion. This could mean that these toxins interact with the lipid membrane too as they modulate the VGSC, because effects appear within 20 to 50 s of application. This mechanism of action would in turn suggest the possibility that CcoTx2 does dissociate from the channel at high voltages (Fig. 5C) but stays close to the VGSC and remains bound to the membrane so that it can bind again thereafter.

ET Analysis. The ET analysis of related ICK toxin sequences outlines the potential importance of basic residues

and particularly of amino acids in loops 1 and 4 (Fig. 7). When linking this theoretical model with the result of the mutant cycle analysis of SGTx1, an excellent correlation is seen (Wang et al., 2004). Mutagenesis of SGTx1 outlined the crucial importance of residues in loops 1 and 4, in particular Arg3, Arg22, and Asp24. These residues are all singled out by our ET analysis. Mutagenesis, however, points to the importance of aromatic residues in loops 1 and 4 in defining the hydrophobic contact surface of the toxin, whereas the ET analysis seems to be biased toward the more basic residues. This is exemplified by the strong basic node that is present in face A of the toxin. Consistent with the hydrophobic patch contact hypothesis, our ET analysis indicates that face A of the toxins encompasses all important residues, whereas face B includes a leucine at position 3 that can make a pharmacological or structural contribution. Clearly, an ET analysis based solely on a combination of primary sequences of peptides is not sufficient to completely predict the crucial determinants of toxin function. However, ET analysis can be useful in orienting mutagenesis studies in toxins from which little is known regarding their interaction surface.

References

Bosmans F, Aneiros A, and Tytgat J (2002) The sea anemone Bunodosoma granulifera contains surprisingly efficacious and potent insect-selective toxins. *FEBS Lett* **532:**131–134.

Bourinet E, Stotz SC, Spaetgens RL, Dayanithi G, Lemos J, Nargeot J, and Zamponi GW (2001) Interaction of SNX482 with domains III and IV inhibits activation gating of alpha(1E) (Ca$_V$2.3) calcium channels. *Biophys J* **81:**79–88.

Craik DJ, Daly NL, and Waine C (2001) The cystine knot motif in toxins and implications for drug design. *Toxicon* **39:**43–60.

Craner MJ, Newcombe J, Black JA, Hartle C, Cuzner ML, and Waxman SG (2004) Molecular changes in neurons in multiple sclerosis: altered axonal expression of Nav1.2 and Nav1.6 sodium channels and Na$^+$/Ca^{2+} exchanger. *Proc Natl Acad Sci USA* **101:**8168–8173.

Escoubas P, De Weille JR, Lecoq A, Diochot S, Waldmann R, Champigny G, Moinier D, Menez A, and Lazdunski M (2000a) Isolation of a tarantula toxin specific for a class of proton-gated Na$^+$ channels. *J Biol Chem* **275:**25116–25121.

Escoubas P, Diochot S, Celerier ML, Nakajima T, and Lazdunski M (2002) Novel tarantula toxins for subtypes of voltage-dependent potassium channels in the Kv2 and Kv4 subfamilies. *Mol Pharmacol* **62:**48–57.

Escoubas P, Diochot S, and Corzo G (2000b) Structure and pharmacology of spider venom neurotoxins. *Biochimie* **82:**893–907.

Escoubas P and Rash L (2004) Tarantulas: eight-legged pharmacists and combinatorial chemists. *Toxicon* **43:**555–574.

French RJ and Terlau H (2004) Sodium channel toxins–receptor targeting and therapeutic potential. *Curr Med Chem* **11:**3053–3064.

Head C and Gardiner M (2003) Paroxysms of excitement: sodium channel dysfunction in heart and brain. *Bioessays* **25:**981–993.

Julius D and Basbaum AI (2001) Molecular mechanisms of nociception. *Nature (Lond)* **413:**203–210.

Kayano T, Noda M, Flockerzi V, Takahashi H, and Numa S (1988) Primary structure of rat brain sodium channel III deduced from the cDNA sequence. *FEBS Lett* **228:**187–194.

Lee CW, Kim S, Roh SH, Endoh H, Kodera Y, Maeda T, Kohno T, Wang JM, Swartz KJ, and Kim JI (2004) Solution structure and functional characterization of SGTx1, a modifier of Kv2.1 channel gating. *Biochemistry* **43:**890–897.

Lewis RJ and Garcia ML (2003) Therapeutic potential of venom peptides. *Nat Rev Drug Discov* **2:**790–802.

Li D, Xiao Y, Hu W, Xie J, Bosmans F, Tytgat J, and Liang S (2003) Function and solution structure of hainantoxin-I, a novel insect sodium channel inhibitor from the Chinese bird spider Selenocosmia hainana. *FEBS Lett* **555:**616–622.

Li D, Xiao Y, Xu X, Xiong X, Lu S, Liu Z, Zhu Q, Wang M, Gu X, and Liang S (2004) Structure-activity relationships of hainantoxin-IV and structure determination of active and inactive sodium channel blockers. *J Biol Chem* **279:**37734–37740.

Li-Smerin Y and Swartz KJ (1998) Gating modifier toxins reveal a conserved structural motif in voltage-gated Ca^{2+} and K$^+$ channels. *Proc Natl Acad Sci USA* **95:**8585–8589.

McDonough SI, Lampe RA, Keith RA, and Bean BP (1997) Voltage-dependent inhibition of N- and P-type calcium channels by the peptide toxin ω-grammotoxin-SIA. *Mol Pharmacol* **52:**1095–1104.

Middleton RE, Warren VA, Kraus RL, Hwang JC, Liu CJ, Dai G, Brochu RM, Kohler MG, Gao YD, Garsky VM, et al. (2002) Two tarantula peptides inhibit activation of multiple sodium channels. *Biochemistry* **41:**14734–14747.

Nassar MA, Stirling LC, Forlani G, Baker MD, Matthews EA, Dickenson AH, and Wood JN (2004) Nociceptor-specific gene deletion reveals a major role for Nav1.7 (PN1) in acute and inflammatory pain. *Proc Natl Acad Sci USA* **101:**12706–12711.

Newcomb R, Szoke B, Palma A, Wang G, Chen X, Hopkins W, Cong R, Miller J, Urge L, Tarczy-Hornoch K, et al. (1998) Selective peptide antagonist of the class E calcium channel from the venom of the tarantula *Hysterocrates gigas. Biochemistry* **37:**15353–15362.

Peng K, Shu Q, Liu Z, and Liang S (2002) Function and solution structure of huwentoxin-IV, a potent neuronal tetrodotoxin (TTX)-sensitive sodium channel antagonist from Chinese bird spider Selenocosmia huwena. *J Biol Chem* **277:** 47564–47571.

Possani LD, Becerril B, Delepierre M, and Tytgat J (1999) Scorpion toxins specific for Na$^+$-channels. *Eur J Biochem* **264:**287–300.

Rash LD and Hodgson WC (2002) Pharmacology and biochemistry of spider venoms. *Toxicon* **40:**225–254.

Smith JJ, Alphy S, Seibert AL, and Blumenthal KM (2005) Differential phospholipid binding by site 3 and site 4 toxins: Implications for structural variability between voltage-sensitive sodium channel domains. *J Biol Chem.* **25:**11127–11133.

Smith RD and Goldin AL (1998) Functional analysis of the rat I sodium channel in Xenopus oocytes. *J Neurosci* **18:**811–820.

Sollod BL, Wilson D, Zhaxybayeva O, Gogarten JP, Drinkwater R, and King GF (2005) Were arachnids the first to use combinatorial peptide libraries? *Peptides* **26:**131–139.

Suchyna TM, Johnson JH, Hamer K, Leykam JF, Gage DA, Clemo HF, Baumgarten CM, and Sachs F (2000) Identification of a peptide toxin from Grammostola spatulata spider venom that blocks cation-selective stretch-activated channels. *J Gen Physiol* **115:**583–598.

Swanson R, Marshall J, Smith JS, Williams JB, Boyle MB, Folander K, Luneau CJ, Antanavage J, Oliva C, Buhrow SA and et al. (1990) Cloning and expression of cDNA and genomic clones encoding three delayed rectifier potassium channels in rat brain. *Neuron* **4:**929–939.

Swartz KJ and MacKinnon R (1995) An inhibitor of the Kv2.1 potassium channel isolated from the venom of a Chilean tarantula. *Neuron* **15:**941–949.

Takahashi H, Kim JI, Min HJ, Sato K, Swartz KJ, and Shimada I (2000) Solution structure of hanatoxin1, a gating modifier of voltage-dependent K$^+$ channels: common surface features of gating modifier toxins. *J Mol Biol* **297:**771–780.

Wang JM, Roh SH, Kim S, Lee CW, Kim JI, and Swartz KJ (2004) Molecular surface of tarantula toxins interacting with voltage sensors in K(v) channels. *J Gen Physiol* **123:**455–467.

Wang SY and Wang GK (2003) Voltage-gated sodium channels as primary targets of diverse lipid-soluble neurotoxins. *Cell Signal* **15:**151–159.

Winterfield JR and Swartz KJ (2000) A hot spot for the interaction of gating modifier toxins with voltage-dependent ion channels. *J Gen Physiol* **116:**637–644.

Wood JN, Boorman JP, Okuse K, and Baker MD (2004) Voltage-gated sodium channels and pain pathways. *J Neurobiol* **61:**55–71.

Xiao Y and Liang S (2003) Inhibition of neuronal tetrodotoxin-sensitive Na$^+$ channels by two spider toxins: hainantoxin-III and hainantoxin-IV. *Eur J Pharmacol* **477:**1–7.

Xiao Y, Tang J, Yang Y, Wang M, Hu W, Xie J, Zeng X, and Liang S (2004) Jingzhaotoxin-III, a novel spider toxin inhibiting activation of voltage-gated sodium channel in rat cardiac myocytes. *J Biol Chem* **279:**26220–26226.

Yu FH and Catterall WA (2003) Overview of the voltage-gated sodium channel family. *Genome Biol* **4:**207.

Yu FH, Westenbroek RE, Silos-Santiago I, McCormick KA, Lawson D, Ge P, Ferriera H, Lilly J, DiStefano PS, Catterall WA, et al. (2003) Sodium channel beta4, a new disulfide-linked auxiliary subunit with similarity to beta2. *J Neurosci* **23:**7577–7585.

Zhu S, Huys I, Dyason K, Verdonck F, and Tytgat J (2004) Evolutionary trace analysis of scorpion toxins specific for K-channels. *Proteins* **54:**361–370.

Address correspondence to: Jan Tytgat, University of Leuven, Laboratory of Toxicology, Van Evenstraat 4, Leuven 3000, Belgium. E-mail: jan.tytgat@pharm.kuleuven.be